RSC Advances

PAPER

View Article Online
View Journal | View Issue

Cite this: *RSC Adv.*, 2014, **4**, 50373

Azopyridine-functionalized benzoxazine with $Zn(ClO_4)_2$ form high-performance polybenzoxazine stabilized through metal–ligand coordination

Mohamed Gamal Mohamed,[a] Wei-Chen Su,[a] Yung-Chih Lin,[a] Chih-Feng Wang,[d] Jem-Kun Chen,[e] Kwang-Un Jeong[f] and Shiao-Wei Kuo*[abc]

In this study, we prepared a benzoxazine monomer (Azopy-BZ) that features azobenzene and pyridine units through the reaction of paraformaldehyde, aniline, and 4-(4-hydroxphenylazo)pyridine (Azopy-OH), which is obtained through a diazonium reaction of 4-aminopyridine with phenol in the presence of sodium nitrite and NaOH. The azobenzene and pyridine groups in the benzoxazine monomer play the following two roles: (i) allowing photoisomerization between the planar *trans* form and the nonplanar *cis* form of the azobenzene unit (characterized using UV-vis spectroscopy and contact angle analyses) and (ii) serving as a catalyst that accelerated the ring opening polymerization of the benzoxazine units, which was characterized by the exothermic peak shifting to a lower temperature during differential scanning calorimetry (DSC) analyses. The curing temperature of the model benzoxazine 3-phenyl-3,4-dihydro-2*H*-benzoxazine (Pa-type) was 263 °C; it decreased to 208 °C for Azopy-BZ, presumably because of the basicity of the azobenzene and pyridine groups. Blending with zinc perchlorate [$Zn(ClO_4)_2$] not only improved the thermal properties, as determined through dynamic mechanical analysis (DMA), due to physical crosslinking of the pyridine units through zinc cation coordination in a metal–ligand bonding mode, but also further facilitated the ring opening polymerization to occur at a temperature of only 130 °C (DSC). Thus, the presence of $Zn(ClO_4)_2$ overcame the problem of high temperature curing (*ca.* 180–210 °C) required for traditional polybenzoxazines. Introducing the azobenzene and pyridine units and the zinc salt into this polybenzoxazine system provided a multifunctional material that exhibited photoisomerization-based tuning of its surface properties, accelerated ring opening polymerization of its oxazine rings, and increasing physical crosslinking density, through metal–ligand interactions, to enhance its thermal properties.

Received 8th August 2014
Accepted 22nd September 2014

DOI: 10.1039/c4ra08381d

www.rsc.org/advances

Introduction

1,3-Benzoxazines are receiving considerable attention because of their promising practical applications as monomers for high performance materials.[1–6] Their facile and versatile syntheses from relatively abundant materials (*e.g.*, phenols, amines, formaldehyde) is also attractive from the view point of developing novel benzoxazines bearing a variety of functional groups.[7–17] Some of these functional groups serve as reactive sites to increase the degree of crosslinking, thereby varying the thermal and mechanical properties of the obtained polybenzoxazines to fulfill specific requirements. Because the chemical structure of a polybenzoxazine is similar to that of a traditional phenolic resin, polybenzoxazines possess good heat resistance, good flame retardancy, good mechanical properties, low dielectric constants, dimensional stability, low water absorption, and low surface free energy.[1,18–26] As a result, polybenzoxazines have potential uses as matrix resins for carbon fiber-reinforced plastics, adhesives, and electronic materials (*e.g.*, rigid printed circuit boards). Nevertheless, polybenzoxazines do have some unattractive properties, including high curing temperatures for their ring opening polymerizations, brittleness, and moderate glass transition temperatures (T_g) that are not sufficiently high for applications under harsh

[a]*Department of Materials and Optoelectronic Science, National Sun Yat-Sen University, Kaohsiung, Taiwan*
[b]*Department of Medicinal and Applied Chemistry, Kaohsiung Medical University, Kaohsiung, Taiwan*
[c]*School of Chemical Engineering, East China University of Science and Technology, Shanghai, China. E-mail: kuosw@faculty.nsysu.edu.tw*
[d]*Department of Materials Science and Engineering, I-Shou University, Kaohsiung, Taiwan*
[e]*Department of Polymer-Nano Science and Technology, Chonbuk National University, Jeonju, Korea*
[f]*Department of Materials Science and Engineering, National Taiwan University of Science and Technology, Taiwan*

conditions.[1,23,27] Many approaches have been reported to overcome these shortcomings. For example, the mechanical and thermal properties of the benzoxazine can be improved significantly after blending with various polymers (*e.g.*, epoxy,[28,29] polyurethane,[30,31] polyimide[32]) or through copolymerization. In addition, the preparation of specifically designed novel polybenzoxazines or high-molecular-weight benzoxazines, featuring another polymerizable group (*e.g.*, ethynyl,[33] phenylethynyl,[34] nitrile,[35] propargyl,[36] allyl[37]) or hydrogen bonding functional group,[38,39] can be an effective means of enhancing thermal properties.

Another application of functionalized benzoxazine monomers is their combination with inorganic materials (*e.g.*, clay,[40–42] polyhedral oligomeric silsesquioxane (POSS),[43–47] carbon nanotubes,[48,49] graphene[50]) to fabricate nanocomposites, stabilized through attractive interactions between the polar functional groups of the monomer units and the inorganic surfaces. For example, Yagci *et al.* demonstrated the surface functionalization of magnetite nanoparticles with a benzoxazine bearing a carboxyl moiety, and they also developed a polybenzoxazine/montmorillonite nanocomposite by using a benzoxazine bearing a 4-pyridyl moiety as a key material.[40,41]

Combining metal ions with benzoxazines is also an interesting means of preparing new high-performance polybenzoxazines. Endo *et al.* reported a novel 1,3-benzoxazine bearing a 4-aminopyridyl moiety, synthesized from 4-aminopyridine, *p*-cresol, and paraformaldehyde, with acetic acid added to neutralize the basicity of the system. The introduction of the 4-aminopyridyl moiety resulted in a polymer exhibiting high affinity toward metal ions [*e.g.*, copper(II), cobalt(II)], leading to the production of polymer–metal complexes in the form of insoluble colored precipitates.[41,51] Furthermore, among known photoresponsive molecules, azobenzene derivatives are the most popular for photo switching applications[52,53] because they can photoisomerize reversibly between their planar *trans* form and nonplanar *cis* form upon irradiation with light. Azobenzene derivatives have two major advantages over other molecules when used as photoswitches: their chemical

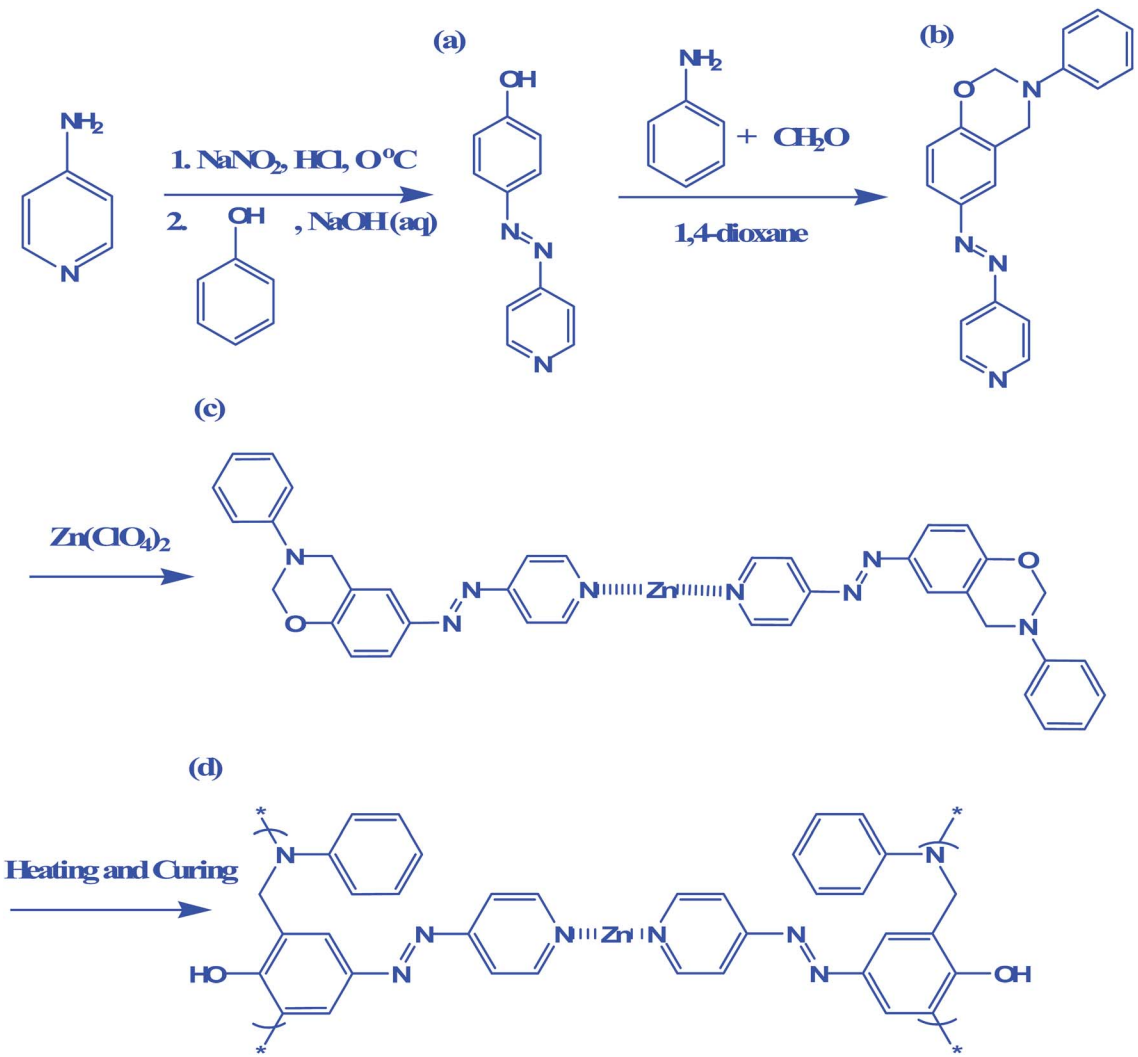

Scheme 1 (a and b) Syntheses of (a) Azopy-OH and (b) Azopy-BZ. (c) Metal–ligand coordination of $Zn(ClO_4)_2$ and Azopy-BZ; (d) possible structure of $Zn(ClO_4)_2$/poly(Azopy-BZ) complexes.

synthesis is relatively simple (indeed, some are commercially available) and they exhibit chemical stability, allowing repeated *trans*-to-*cis* photoisomerizations without decomposition—even under aqueous conditions. In addition, *trans*-to-*cis* isomerization occurs with irradiation near 350 nm, while *cis*-to-*trans* isomerization is induced by harmless visible light.

In this study, we prepared a benzoxazine derivative, Azopy-BZ, featuring an azobenzene/pyridine functional group. First, we prepared 4-(4-hydroxphenyleazo)pyridine (Azopy-OH) through a diazonium reaction of 4-aminopyridine with phenol in the presence of NaOH [Scheme 1(a)]. Next, we obtained Azopy-BZ through the reaction of Azopy-OH, paraformaldehyde, and aniline in 1,4-dioxane [Scheme 1(b)]. We then investigated the physical properties and specific interactions of Azopy-BZ when blended with various weight ratios of zinc perchlorate [$Zn(ClO_4)_2$] before [Scheme 1(c)] and after [Scheme 1(d)] thermal curing. We employed differential scanning calorimetry (DSC), Fourier transform infrared (FTIR) spectroscopy, dynamic mechanical analysis (DMA), and contact angle analyses to examine the thermal behavior, specific interactions, and surface properties of these materials.

Experimental section

Materials

4-Aminopyridine, paraformaldehyde (96%), sodium nitrite (99%), hydrochloric acid (*ca.* 37%), aniline (99.8%), EtOAc, tetrahydrofuran, and hexane were purchased from Acros. NaOH and 1,4-dioxane were obtained from Aldrich, as was zinc perchlorate hexahydrate [$Zn(ClO_4)_2 \cdot 6H_2O$], which was dried in a vacuum oven at 70 °C for 24 h prior to use.

Azopy-OH

A solution of phenol (5.0 g, 53 mmol) and sodium nitrite (4.0 g, 58 mmol) in 10% (w/w) aqueous NaOH (20 mL) was added dropwise to a solution of 4-aminopyridine (6.0 g, 64 mmol) in 7.3 N HCl (45 mL) at 0 °C. The mixture was adjusted to pH 6 through the addition 10% aqueous NaOH. The orange precipitate was filtered off, washed with water, dried and recrystallized (acetone/water) to give the product (3.5 g, 35%). M.p. (DSC): 263–265 °C. ^{1}H NMR (δ, DMSO-d_6): 6.98 (d, 2H), 7.67 (d, 2H), 7.88 (d, 2H), 8.77 (d, 2H), 10.59 (s, 1H). ^{13}C NMR (δ, DMSO-d_6): 162.29, 156.81, 151.32, 145.24, 125.77, 116.18, 115.77. IR (KBr, cm^{-1}): 3204–3463 (OH).

Azopy-BZ

A solution of aniline (1.03 g, 11 mmol) in 1,4-dioxane (25 mL) was added portion wise to a solution of paraformaldehyde (0.66 g, 22 mmol) in 1,4-dioxane (100 mL) in a 250 mL flask cooled in an ice bath. The mixture was stirred for 20 min at a temperature below 5 °C, and then a solution of Azopy-OH (2.0 g, 10 mmol) in 1,4-dioxane (30 mL) was added. The mixture was heated under reflux at 90–95 °C for 24 h. After cooling, rotary evaporation of the solvent gave a viscous residue that was dissolved in EtOAc (100 mL) and washed several times with 5% $NaHCO_3$ and finally with distilled water. The organic phase was dried ($MgSO_4$), filtered, and concentrated under vacuum to afford an orange residue, which was purified through column chromatography (SiO_2; *n*-hexane/THF, 1 : 1) to give an orange powder (65%). M.p. (DSC): 163 °C. ^{1}H NMR (δ, DMSO-d_6): 4.82 (s, 2H, CH_2N), 5.61 (s, 2H, OCH_2N), 6.88 (s, 1H, CH), 6.94 (s, 1H), 6.96 (d, 2H), 7.16 (d, 2H), 7.23 (d, 2H), 7.84 (d, 2H), 8.79 (d, 2H). ^{13}C NMR (δ, DMSO-d_6): 48.59 (CCH_2N), 79.79 (OCH_2N), 115.76–158.32 (aromatic). IR (KBr, cm^{-1}): 1230 (asymmetric C–O–C stretching); 1341 (CH_2 wagging); 915, 923, and 1490 (trisubstituted benzene ring); 1441 (stretching of *trans* N=N).

Characterization

^{1}H and ^{13}C nuclear magnetic resonance (NMR) spectra were recorded using an INOVA 500 instrument with DMSO as the solvent and TMS as the external standard. Chemical shifts are reported in parts per million (ppm). FTIR spectra of the polymer films were recorded using a Bruker Tensor 27 FTIR spectrophotometer and the conventional KBr disk method; moreover, note that 32 scans were collected at a spectral resolution of 4 cm^{-1}. The films tested in this study were sufficiently thin to obey the Beer–Lambert law. FTIR spectra recorded at elevated temperatures were obtained from a cell mounted inside the temperature-controlled compartment of the spectrometer. Dynamic curing kinetics was determined using a TA Q-20 differential scanning calorimeter operated under a N_2 atmosphere. The sample (*ca.* 5 mg) was placed in a sealed aluminum sample pan. Dynamic curing scans were recorded from 30 to 350 °C at a heating rate of 20 °C min^{-1}. The thermal stability of the samples was measured using a TG Q-50 thermogravimetric analyzer operated under a N_2 atmosphere. The cured sample (*ca.* 5 mg) was placed in a Pt cell and heated at a rate of 20 °C min^{-1} from 30 to 800 °C under a N_2 flow rate of 60 mL min^{-1}. DMA was performed using a PerkinElmer instrument DMA 8000 apparatus operated in tension mode and for the preparation of the samples for DMA; moreover, the sample powder was sandwiched in the middle of a single cantilever and the bending was measured at temperatures from room temperature to 250 °C. Analyses of the loss tangent (tan δ) were recorded automatically by the system, and the heating rate and frequency were fixed at 2 °C min^{-1} and 1 Hz, respectively. UV-vis spectra were recorded using a Shimadzu mini 1240 spectrophotometer. Photoisomerization of the azobenzene unit was performed using a UV-vis lamp directly at 365 nm (UV, 90 mW cm^{-2}) and through a filter at 400–500 nm (visible, 90 mW cm^{-2}) to generate the light for the *trans*-to-*cis* and *cis*-to-*trans* isomerizations, respectively. The concentration of Azopy-BZ in THF was 10^{-4} M for the UV-vis spectroscopic study. The contact angles of the polymer samples before and after curing were measured at 25 °C using a FDSA Magic Droplet 100 contact angle goniometer interfaced with image capture software after injecting a 5 μL liquid drop. To obtain reliable contact data, at least three droplets were measured at different regions of the same piece of film, with at least two pieces of film being used. Thus, at least six advancing contact angles were averaged for each type of film with each type of solvent. Note that deionized water was used as a standard when measuring the surface properties.

Results and discussion

Synthesis of Azopy-BZ through Mannich reaction of Azopy-OH with aniline and paraformaldehyde

We prepared Azopy-BZ in high purity and high yield, even though it was possible that we might generate various side products, due to the high reactivity of pyridyl and its ability to form a hydrogen bond intramolecularly with phenol groups. Fig. 1 presents the ^{1}H NMR spectra of Azopy-OH and Azopy-BZ. The spectrum of Azopy-OH [Fig. 1(a)] features a signal at 10.58 ppm, corresponding to the proton of the phenolic OH group, with the signals of the aromatic protons of the azobenzene pyridine unit appearing as multiplets in the range of 6.97–8.77 ppm. The spectrum of Azopy-BZ [Fig. 1(b)] features the signals for the CH_2N and OCH_2N bridges of the oxazine unit at 4.82 and 5.61 ppm, respectively. The signal of the proton of the phenolic OH group of Azopy-OH is absent, but the signals of the azobenzene pyridine moiety are present, confirming the successful synthesis of Azopy-BZ.

Fig. 2 presents the ^{13}C NMR spectra of Azopy-OH and Azopy-BZ. The signals of the azobenzene pyridine moiety appear in the range from 115.75 to 158.32 ppm in Fig. 2(a). Two peaks appear at 48.6 and 79.9 ppm in the spectrum of Azopy-BZ in Fig. 2(b), representing the carbon nuclei of the oxazine ring, and the signals of the azobenzene pyridine ring confirm the successful synthesis of Azopy-BZ. Fig. 3 presents the FTIR spectra of Azopy-OH and Azopy-BZ at room temperature and of poly(Azopy-BZ) after thermal curing. The spectrum of Azopy-OH features a sharp signal for the OH group at 3442 cm^{-1} and absorption bands for the aromatic ring at 3025, 1610, and 1571 cm^{-1} [Fig. 3(a)]. In the spectrum of Azopy-BZ [Fig. 3(b)], the signal for the phenolic OH group is absent, but signals are evident for C–C stretching vibrations of the 1,2,4-substituted benzene ring at 1490 and 923 cm^{-1} for the oxazine ring, for asymmetric C–O–C stretching at 1229 cm^{-1}, and for stretching of the *trans* N=N bond at 1440 cm^{-1}. These spectroscopic features confirmed the successful synthesis of Azopy-BZ. Fig. 3(c) presents the FTIR spectrum recorded after thermal curing of pure Azopy-BZ. The characteristic absorption bands at 1490 and 923 cm^{-1} for the trisubstituted aromatic ring of Azopy-BZ disappeared after thermal curing with the former shifting to 1502 cm^{-1} for the tetrasubstituted aromatic ring of poly(Azopy-BZ). The broad absorption bands in the range of 2600–3500 cm^{-1} in Fig. 3(c) represent three different kinds of hydrogen bonding interactions: intramolecular [$O^{-}\cdots H-N^{+}$] hydrogen bonding (*ca.* 2800 cm^{-1}), intramolecular [O–H···N] hydrogen bonding (*ca.* 3200 cm^{-1}), and intermolecular [O–H···O] hydrogen bonding (*ca.* 3342 cm^{-1}); the identities of these signals have been reported previously.[18,54]

Thermal Polymerization of Azopy-BZ

We used DSC to determine the curing behavior of pure Azopy-BZ (Fig. 4). The DSC trace of uncured Azopy-BZ featured a sharp

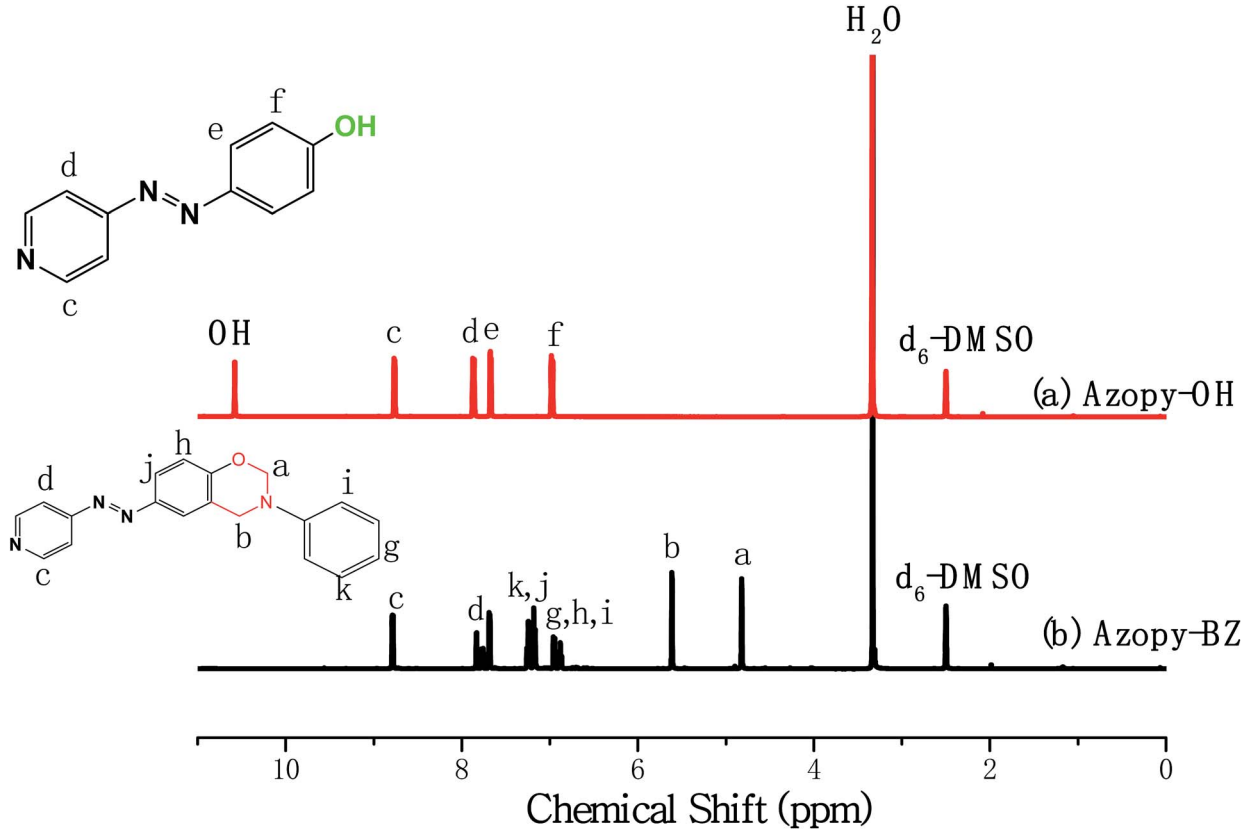

Fig. 1 ^{1}H NMR spectra of (a) Azopy-OH and (b) Azopy-BZ.

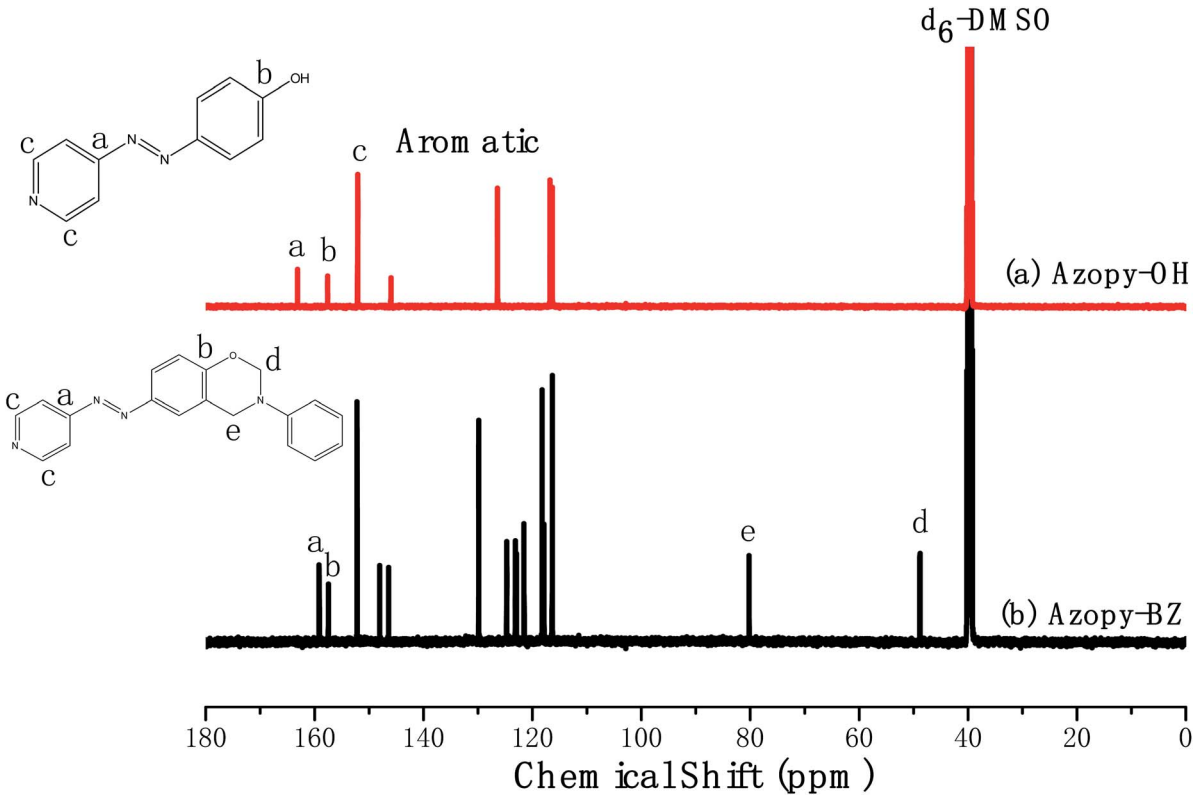

Fig. 2 ^{13}C NMR spectra of (a) Azopy-OH and (b) Azopy-BZ.

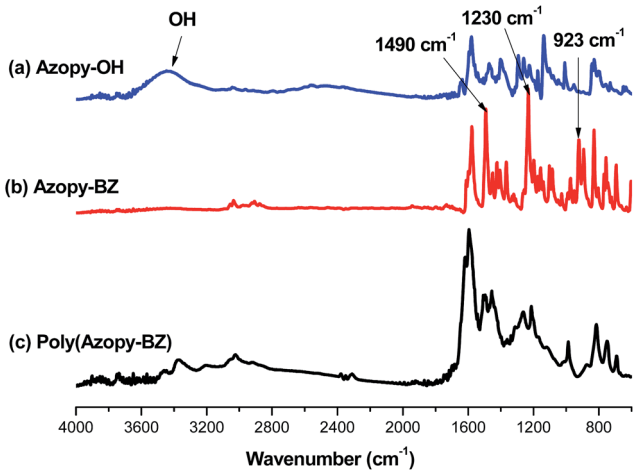

Fig. 3 FTIR spectra of (a) Azopy-OH, (b) Azopy-BZ, and (c) poly(Azopy-BZ), recorded at room temperature.

melting peak at 163 °C, revealing the high purity of the Azopy-BZ monomer. A sharp exothermic peak, which we attribute to the ring opening polymerization of Azopy-BZ, appeared with its onset at 198 °C and its maximum at 208 °C; it had a reaction heat of 579 J g^{-1}. The curing temperature for Azopy-BZ (208 °C) shifted from 263 °C for conventional 3-phenyl-3,4-dihydro-2*H*-benzooxazine (Pa-type),[1] presumably because of the basicity of the azo and pyridyl groups, suggesting that the azobenzene and pyridine moieties acted as basic catalysts that contributed to the lower polymerization temperature. After thermal curing of pure Azopy-BZ at 110 °C, the first melting peak was absent from the DSC curve, with the intensity of the exotherm decreasing upon increasing the curing temperature, almost disappearing after thermal curing at temperatures between 150 and 180 °C. Fig. 5 shows FTIR spectra of Azopy-BZ after various curing stages. Upon increasing the curing temperature, we observed a decrease in the intensities of the characteristic absorption bands of the benzoxazine unit at 923 cm^{-1} (C–O–C symmetric), 1230 cm^{-1} (C–O–C asymmetric), and 1490 cm^{-1}.[1] After curing at 180 °C, these characteristic absorption bands had disappeared completely, suggesting that ring opening of the benzoxazine units had reached completion. In addition, after curing at 150 °C, we observed a new absorption band at 2800–3400 cm^{-1}, which is consistent with the formation of a phenolic OH group. These features are consistent with the progress of the ring opening polymerization of Azopy-BZ during thermal curing. Fig. 6 shows TGA thermograms of pure Azopy-BZ before and after thermal curing at 60, 110, 150, and 180 °C under N_2. The thermal stability, the decomposition temperature (10 wt% loss), and the char yield all decreased after curing at 60 and 110 °C, presumably because of loss of the crystal structure at these curing temperatures, consistent with the DSC traces in Fig. 4. Further increase in the curing temperature to 150 and 180 °C caused the decomposition temperature and char yield to increase, which is consistent with increased crosslinking densities enhancing the thermal stabilities of the resulting poly(Azopy-BZ) species.

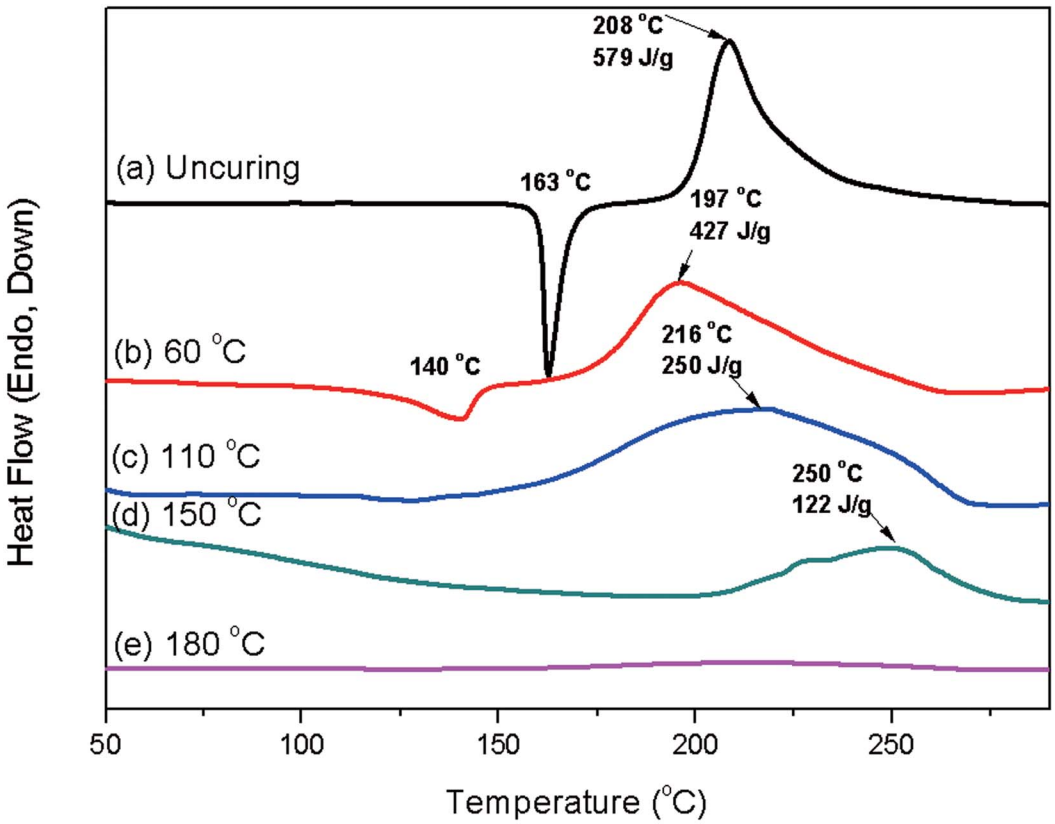

Fig. 4 DSC thermograms of Azopy-BZ, recorded after each curing stage.

Photoisomerization of azopyridine chromophore in Azopy-BZ

Fig. 7 presents UV-vis absorption spectra, revealing the photo-isomerization of the azopyridine chromophore in Azopy-BZ. Fig. 7(a) shows the change in the UV-vis absorption spectra of the Azopy-BZ solution upon irradiation with UV light at 365 nm. The maximum absorption at 360 nm was due to the π–π* transition of the *trans*-azopyridine group. Upon irradiation with UV light, the intensity of the absorbance at 360 nm decreased gradually, eventually reaching a relatively stable value. At the same time, the intensity of the signal near 333 nm, which we assign to the π–π* transition of the *cis* isomer increased. Eventually, the wavelength of maximum absorption shifted from 360 to 333 nm. These variations are consistent with the *trans*-to-*cis* isomerization of the azopyridine group in Azopy-BZ. Fig. 7(b) reveals the change in the UV-vis absorption spectra of the Azopy-BZ solution upon irradiation with UV light at 443 nm; moreover, the intensity of the absorbance at 360 nm increased gradually until reaching a stable state after 3 min, consistent with *cis*-to-*trans* isomerization of the azopyridine group. Fig. 8 displays the contact angles of water for pure Azopy-BZ before and after its photo-isomerization under a UV lamp at 365 nm, as well as after thermal curing at 60, 110, and 150 °C for 3 h and at 180 °C for 2 h. The water contact angles of Azopy-BZ at room temperature and after thermal curing at 60, 110, and 150 °C were 89°, 95°, 98°, and 101°, respectively, and after thermal curing at 180 °C, it reached 108°. Notably, after *trans*-to-*cis* photoisomerization of Azopy-BZ at 60, 110, 150 and 180 °C, the water contact angles changed completely to 29°, 88°, 97°, and 100°, respectively. The water contact angle of the *trans* isomer of Azopy-BZ (95°) was larger than that of the *cis* isomer of Azopy-BZ (29°) after curing at 60 °C, and this behavior is consistent with the *trans* isomer having a smaller dipole moment and lower surface free energy (and therefore a higher water contact angle) and the *cis* form possesses a bigger dipole moment and higher surface free energy (and therefore a lower water contact angle).[55] The water contact angles increased upon increasing the thermal curing temperature and time for both the *trans* and *cis* isomers, due to increased degrees of intramolecular hydrogen bonding and lower surface free energies after thermal curing of the benzoxazine monomer. FTIR spectra revealed (Fig. 5) that four different types of hydrogen bonds were present upon increasing the curing temperature: intramolecular [$O^{-}\cdots H^{+}N$] hydrogen bonds (2830 cm^{-1}), intramolecular [OH···N] (from the Mannich bridge) hydrogen bonds (3200 cm^{-1}), intermolecular [OH···O] and [OH···N] (from pyridyl) hydrogen bonds (3400–3370 cm^{-1}), and intramolecular [OH···π] hydrogen bonds (3459 cm^{-1}), as has been noted in previous reports.[18,54] As a result, the strong intramolecular [OH···N] hydrogen bonds (from the Mannich bridge) dominated for low surface free energy than the photoisomer of Azopy-BZ monomer, and we also found that the water contact angle of the *trans* isomer remained larger than that of the *cis* isomer after thermal curing.

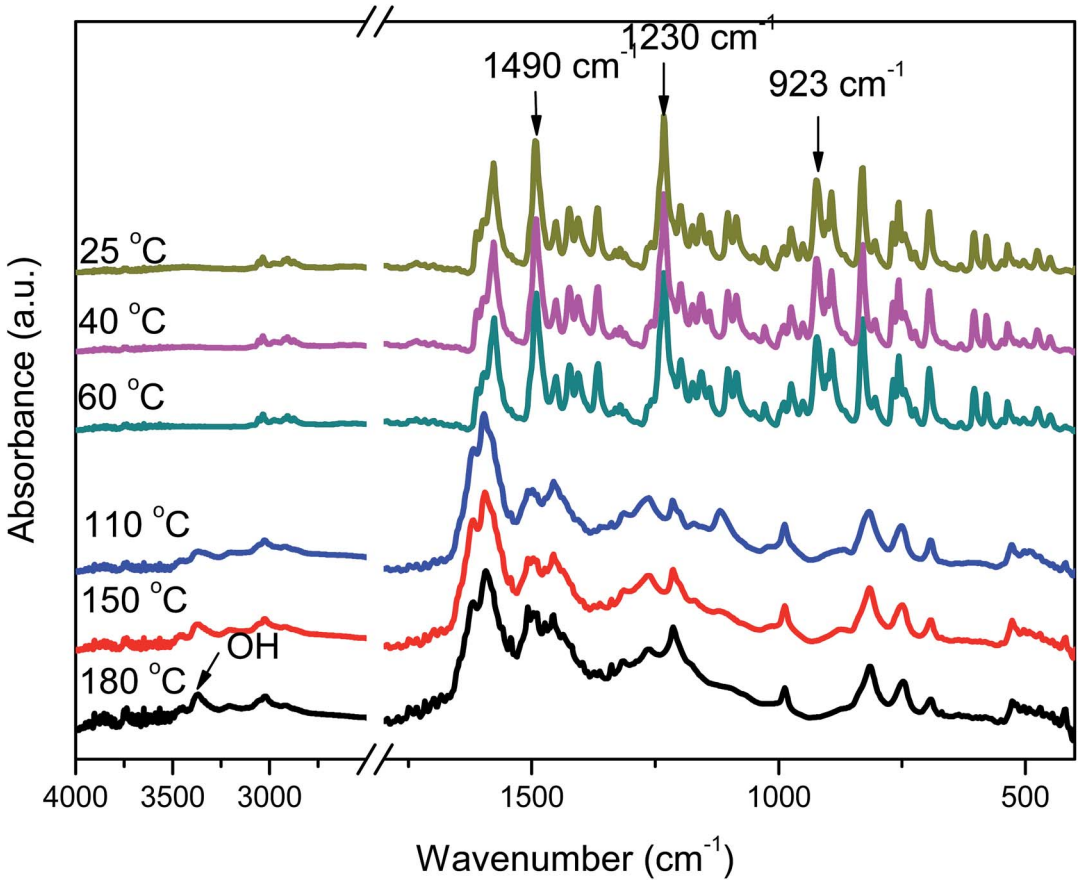

Fig. 5 FTIR spectra of Azopy-BZ, recorded after each curing stage.

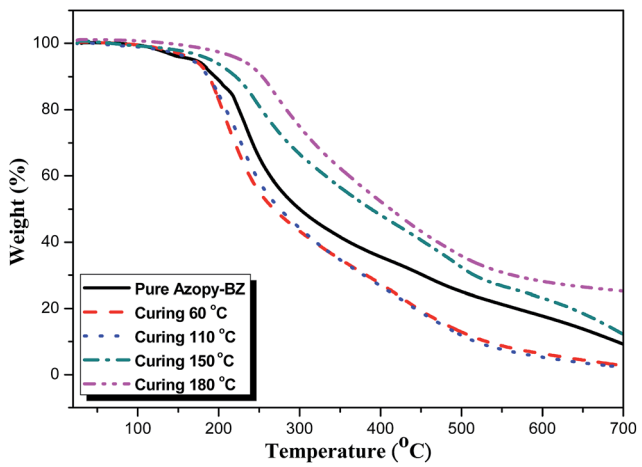

Fig. 6 TGA analyses of Azopy-BZ, recorded after each curing stage.

Thermal Polymerization of Azopy-BZ blended with $Zn(ClO_4)_2$

We used DSC to investigate the thermal curing behavior of pure Azopy-BZ in the presence of various amounts of $Zn(ClO_4)_2$ (Fig. 9). The melting peak disappeared after blending with this zinc salt, indicating that the crystal structure was destroyed upon the interactions of the Zn^{2+} ions with the pyridine or azo groups. Interestingly, prior to thermal curing of the samples containing 1 or 2 wt% of $Zn(ClO_4)_2$, we observed three major curing peaks: near 130, 190, and 233 °C, respectively. The first two curing peaks presumably arose from ring opening of the benzoxazine units coordinated with Zn^{2+} ions, while the latter corresponds to the curing of the non-coordinated benzoxazine units. The curing peak shifted to lower temperature upon the addition of $Zn(ClO_4)_2$, indicating that the Zn^{2+} ions could initiate the ring opening process.[56,57] Ishida *et al.* reported that transition metal salts initiate ring opening, but not the polymerization of Ba-type benzoxazine.[56] The temperature for ring opening of the benzoxazine units shifted from 208 °C in the absence of $Zn(ClO_4)_2$ to 233 °C in its presence because the initial ring opening in the presence of $Zn(ClO_4)_2$ resulted in a certain degree of crosslinking that inhibited the purely thermal curing of the remaining benzoxazine groups. Furthermore, increasing the $Zn(ClO_4)_2$ content to 3–5 wt% caused the second peak at 190 °C to shift completely to 130 °C, thereby increasing the enthalpy of curing at the first peak temperature. Notably, the intensity of the curing peak at 233 °C did not change accordingly, and the total enthalpy of curing of the overall reaction remained relatively unchanged.

Fig. 10(a) presents FTIR spectra of Azopy-BZ blended with various weight ratios of $Zn(ClO_4)_2$ prior to thermal curing. Signals for the stretching of the pyridine ring appeared at 1598, 1490, and 993 cm^{-1}, with these peaks sometimes overlapping

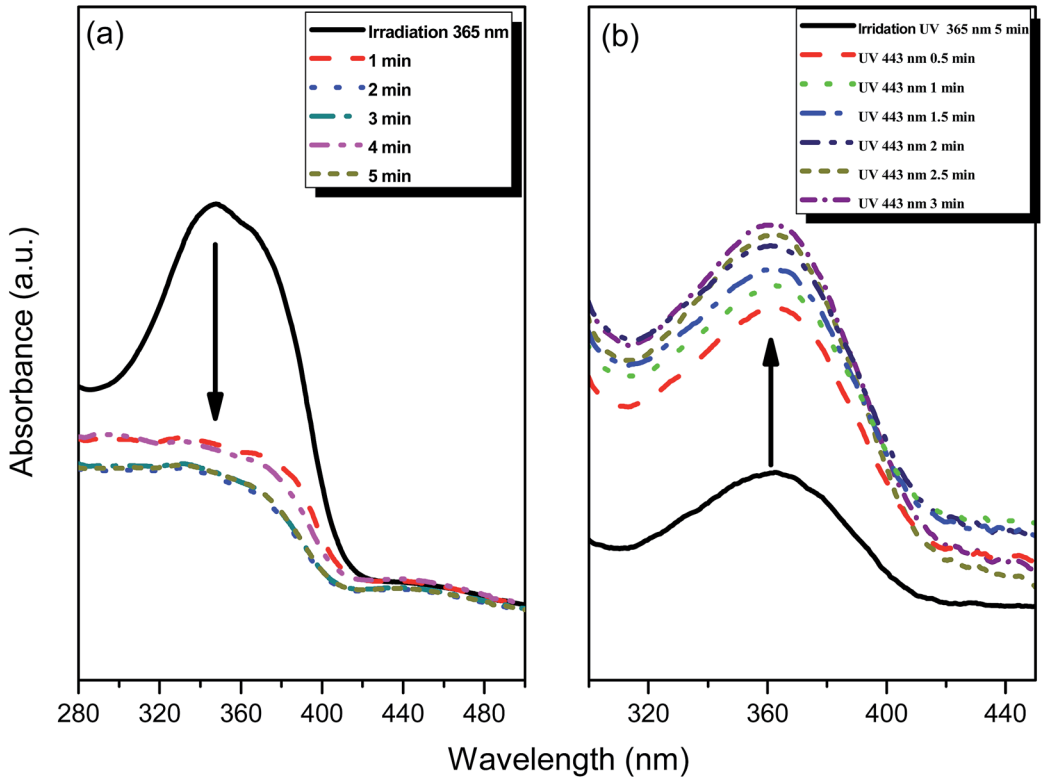

Fig. 7 UV-vis absorption spectra of Azopy-BZ (10^{-4} M in THF) (a) before and (b) after irradiation with UV light at 365 nm for different periods of time.

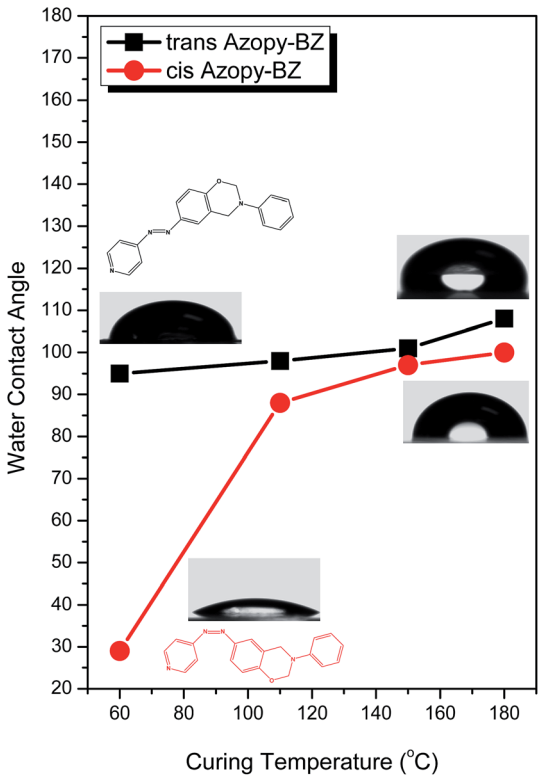

Fig. 8 Water contact angles of Azopy-BZ in its *trans* and *cis* isomeric forms, recorded after each curing stage.

with those representing the aromatic ring; indeed, we observed three major peaks at 1612, 1598, and 1576 cm^{-1} for aromatic stretching of the C=C bonds in the phenyl–O–C, pyridine ring, and phenyl–N–C groups of Azopy-BZ. Upon addition of $Zn(ClO_4)_2$, a new band appeared at 1644 cm^{-1}, the fraction of which increased upon increasing the content of the salt. In a previous study of $Zn(ClO_4)_2$/P4VP blend systems, we found that, upon addition of $Zn(ClO_4)_2$, a similar new band appeared at a relatively high wavenumber, and we assigned this signal as resulting from the Zn^{2+} coordinating to pyridine rings.[58] Pires *et al.* reported that the pyridine units in P4VP behave as π-bonding ligands when coordinated to this cation.[59] Therefore, the higher energy of this new absorption band is the result of the formation of such a coordination complex. Ishida *et al.* found, however, that treatment of benzoxazines with metal salts resulted in an increase in the content of OH groups, indicating the presence of ring-opened structures. They also detected a band at 1654 cm^{-1} after blending with metal salts, tentatively assigned to conjugated C=O groups of possibly quinone-like structures. The OH groups of phenols can be oxidized by metal ions to form quinone structures.[56] The structure of Azopy-BZ, however, differs from that of a Ba-type benzoxazine because it possesses another pyridyl group, which could also interact with $Zn(ClO_4)_2$. To confirm whether such an interaction existed, Fig. 10(b) displays the region of the FTIR spectra featuring the stretching bands of ClO_4^- (from 660 to 600 cm^{-1}) for pure $Zn(ClO_4)_2$ and for various $Zn(ClO_4)_2$/Azopy-BZ blends. In this region, absorptions at 627 and 635 cm^{-1} represent vibrations of

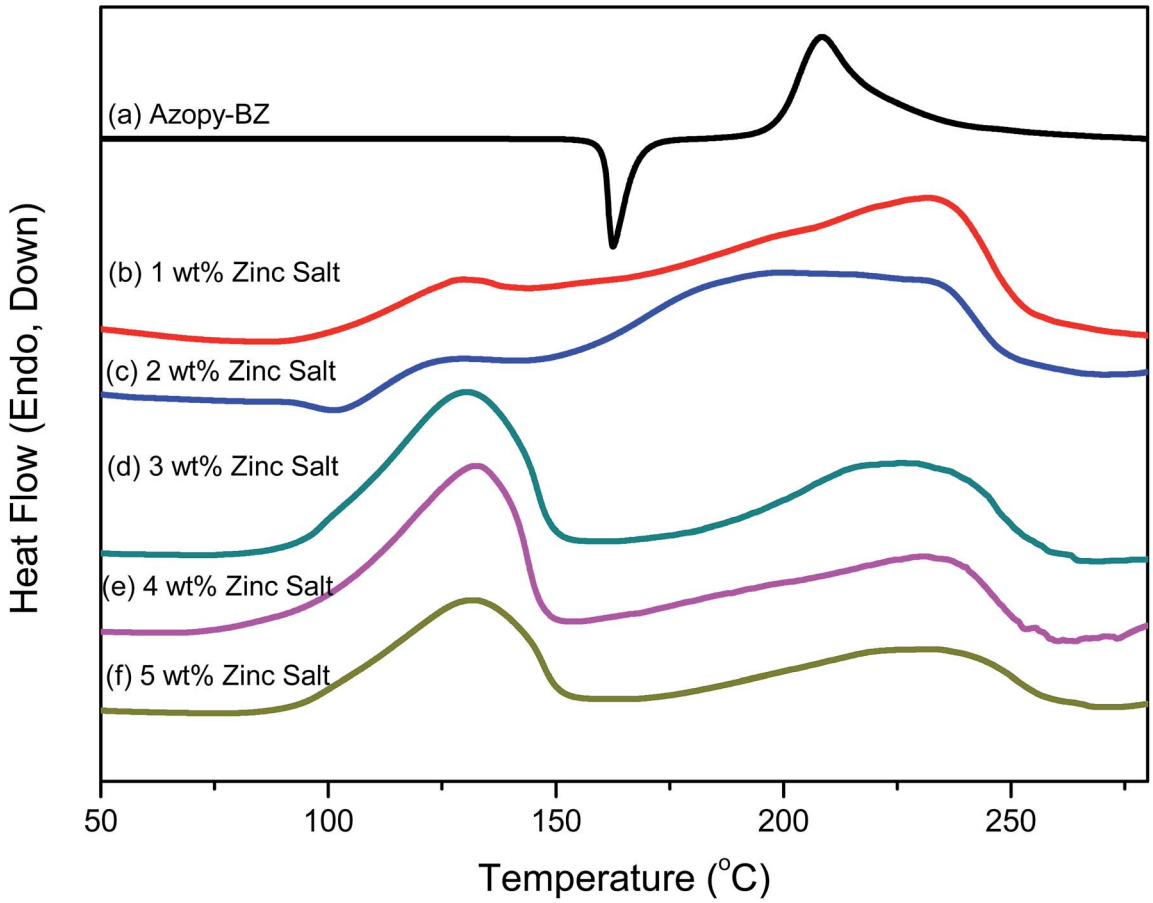

Fig. 9 DSC thermograms of Azopy-BZ in the presence of various amounts of $Zn(ClO_4)_2$.

the free and contacted ClO_4^- ions, respectively.[60] When the concentration of $Zn(ClO_4)_2$ decreased, the band for the contacted ion shifted to lower frequency and became symmetric. We attribute the asymmetric shape of the band for pure $Zn(ClO_4)_2$ to the existence of both free ions and ion pairs. Blending with Azopy-BZ caused the fraction of contacted ions to decrease, consistent with the Zn^{2+} ion interacting with the pyridyl group of Azopy-BZ, causing the fraction of free ClO_4^- anions to increase. We found that the degree of coordination of the pyridine rings increased upon increasing the content of $Zn(ClO_4)_2$.

Fig. 11 presents the thermal curing behavior of Azopy-BZ containing 5 wt% $Zn(ClO_4)_2$. As mentioned above, two major curing peaks appeared at 130 and 233 °C, corresponding to ring opening of the Zn^{2+}-coordinated benzoxazine units and to the original curing of benzoxazine units, respectively. After thermal curing at 60 °C, the intensity of the first exotherm peak decreased, eventually disappearing after thermal curing at 110 °C. The first curing peak shifted to 190 °C, the same curing temperature as that for the second peak of the non-cured Azopy-BZ after blending with 1 wt% $Zn(ClO_4)_2$ (see Fig. 9). After thermal curing at 150 °C, this curing peak also disappeared and shifted to 228 °C, corresponding to the temperature of thermal curing of the original benzoxazine. After thermal curing at 180 °C, the exothermic peaks disappeared completely, suggesting that the ring opening polymerization of Azopy-BZ was complete in the presence of 5 wt% $Zn(ClO_4)_2$.

Fig. 12 presents the FTIR spectra of Azopy-BZ blended with 5 wt% $Zn(ClO_4)_2$ after thermal curing at various temperatures. After thermal curing at 60 °C, the absorption peaks at 1640 and 1092 cm^{-1} disappeared, presumably because of dissociation and the Zn^{2+} ions coordinated with the pyridyl units. After thermal curing at 150 and 180 °C, the characteristic absorption bands of the trisubstituted aromatic rings of the oxazine units at 1490 and 925 cm^{-1} disappeared, with signals for the phenolic OH groups, arising from ring opening, appearing at 1630 and 1512 cm^{-1}. Liu *et al.* reported that the metal salts perform three major steps during the ring opening of benzoxazine. First, the catalyst coordinates with the oxygen and nitrogen atoms of the oxazine ring, and then subsequent electrophilic reactions involve O attack, N attack, and aryl attack, and finally, rearrangement occurs from a phenoxy structure to a phenolic structure.[61] We conclude that the Zn^{2+} ions were effectively coordinated with the oxygen and/or nitrogen atoms during ring opening of the benzoxazine units. In addition, the azopyridine units in Azopy-BZ provided another coordination site to increase the physical crosslinking density, thereby improving the thermal properties after thermal curing.

Finally, we used DMA to investigate the glass transition temperatures of these species. Fig. 13 indicates that the glass

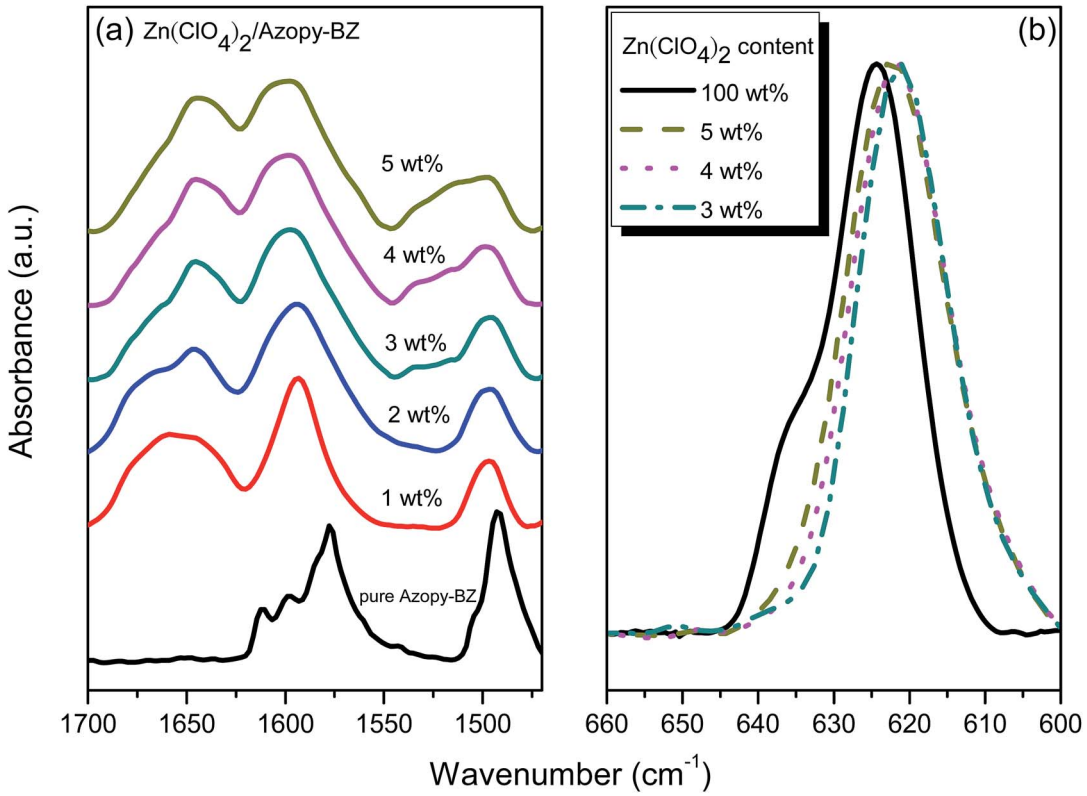

Fig. 10 FTIR spectra of Azopy-BZ in the presence of various amounts of $Zn(ClO_4)_2$, recorded at room temperature.

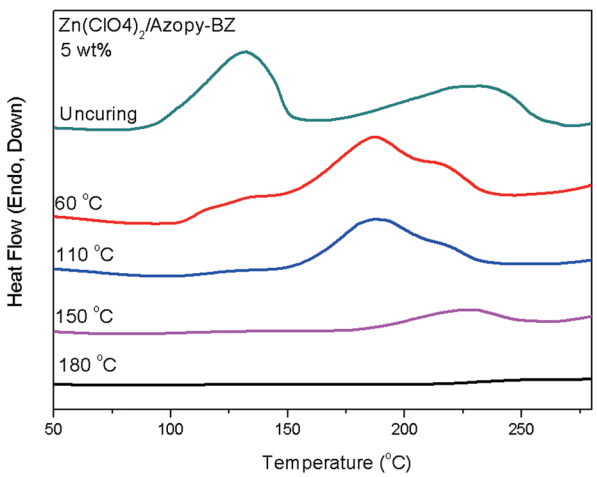

Fig. 11 DSC thermograms of Azopy-BZ in the presence of 5 wt% $Zn(ClO_4)_2$, recorded after each curing stage.

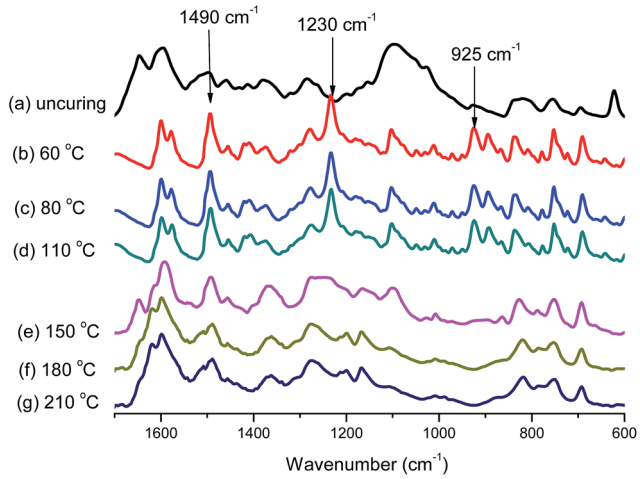

Fig. 12 FTIR spectra of Azopy-BZ in the presence of 5 wt% $Zn(ClO_4)_2$, recorded after each curing stage.

transition temperature of poly(Azopy-BZ) increased from 159 to 198 °C after blending with 5 wt% $Zn(ClO_4)_2$ and thermally curing at 180 °C. The minor peaks at higher temperature may come from another thermal transition for poly(Azopy-BZ) matrix. Clearly, the ionic interactions or ionic cluster formation of ionomers usually resemble physical cross-linking.[58,60,62] The mobility of polymer chains was restricted by such physical cross-links, thereby resulting in higher glass transition temperatures than that of the mother polymer, due to increased the ion–polymer and ion–ion interactions of the polybenzoxazine. Scheme 2 displays some possible modes of metal–ligand coordination in the complex formed between $Zn(ClO_4)_2$ and Azopy-BZ.

Conclusions

In this study, we synthesized an azo/pyridine-functionalized polybenzoxazine. DSC revealed that the exothermic peak for

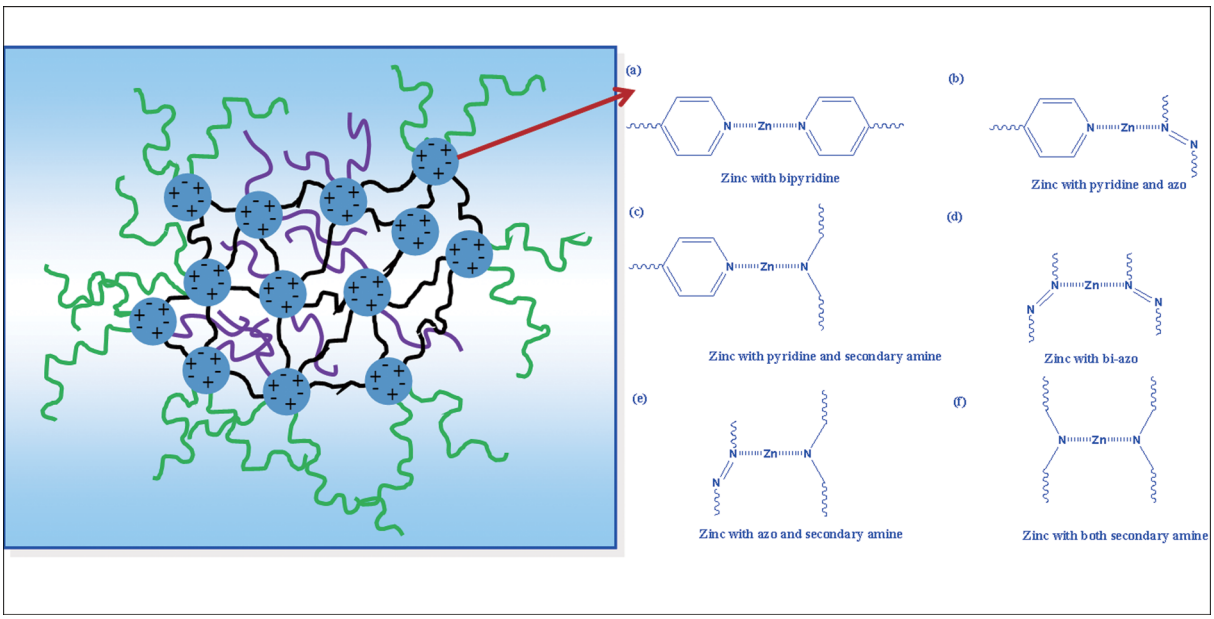

Scheme 2 (Left) Possible morphology of a $Zn(ClO_4)_2$/poly(Azopy-BZ) complex. (Right) Possible modes of metal–ligand coordination between $Zn(ClO_4)_2$ and poly(Azopy-BZ).

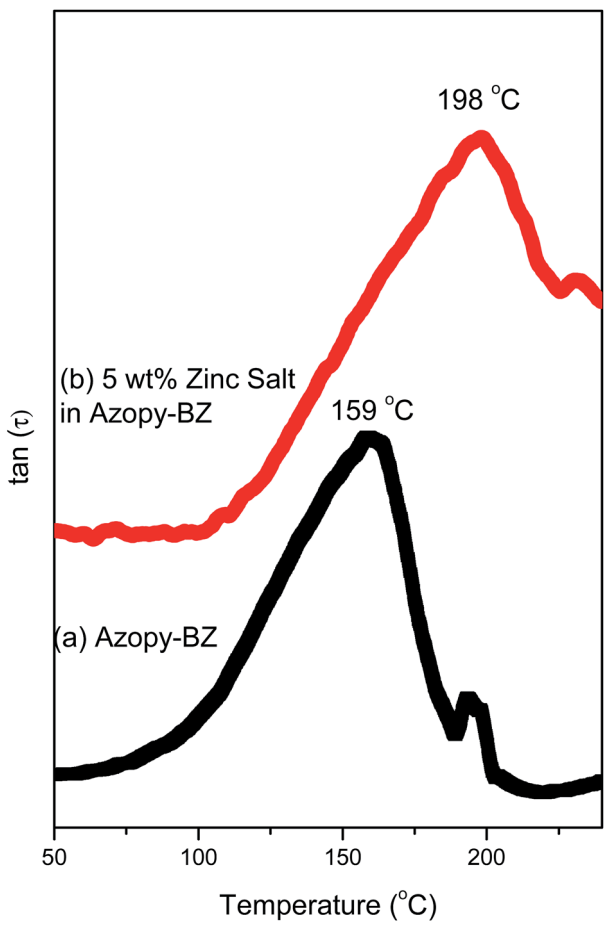

Fig. 13 DMA analyses of (a) pure poly(Azopy-BZ) and (b) $Zn(ClO_4)_2$/poly(Azopy-BZ) = 5/95 after thermal curing.

the ring opening polymerization of benzoxazine itself shifted to lower temperature because the azo and pyridyl groups acted as basic catalysts for the ring opening process. In addition, the azobenzene group also allowed photoisomerization between its planar *trans* form and its nonplanar *cis* form upon irradiation with light, thereby allowing tuning of the surface properties. Furthermore, the azopyridyl moiety in the benzoxazine exhibited high affinity toward Zn^{2+} ions, not only promoting the ring opening polymerization to occur at a relatively low curing temperature (only 130 °C) but also leading to the formation of corresponding polymer–metal complexes and, thereby, improving the thermal properties, based on DMA analyses. Because of such metal–ligand bonding, we predict that such polymers would be useful as metal scavenging materials and as components within polymer/inorganic hybrid materials.

Acknowledgements

This study was supported financially by the National Science Council, Taiwan, Republic of China, under contracts MOST103-2221-E-110-079-MY3 and MOST102-2221-E-110-008-MY3.

References

1 H. Ishida, *"Handbook of Polybenzoxazine"*, ed. Ishida, H. and Agag, T., Elsevier, Amsterdam 2011, ch. 1, p. 1.
2 X. Li and Y. Gu, *Polym. Chem.*, 2011, **2**, 2778–2781.
3 H. Ishida and D. J. Allen, *J. Polym. Sci., Part B: Polym. Phys.*, 1996, **34**, 1019–1030.
4 T. Takeichi, T. Kawauchi and T. Agag, *Polym. J.*, 2008, **40**, 1121–1131.

5 N. N. Ghosh, B. Kiskan and Y. Yagci, *Prog. Polym. Sci.*, 2007, **32**, 1344–1391.
6 C. P. R. Nair, *Prog. Polym. Sci.*, 2004, **29**, 401–498.
7 J. W. Burke, *J. Am. Chem. Soc.*, 1949, **71**, 609–612.
8 T. Agag and T. Takeichi, *Macromolecules*, 2003, **36**, 6010–6017.
9 H. Oie, A. Saudo and T. Endo, *J. Polym. Sci., Part A: Polym. Chem.*, 2010, **48**, 5357–5363.
10 M. Ergin, B. Kiskan, B. Gacal and Y. Yagci, *Macromolecules*, 2007, **40**, 4724–4727.
11 A. Nagai, Y. Kamei, S. Wang, M. Omura, A. Suda, H. Nishida, E. Kawamoto and T. Endo, *J. Polym. Sci., Part A: Polym. Chem.*, 2008, **46**, 2316–2325.
12 B. Kiskan, G. Demirary and Y. Yagci, *J. Polym. Sci., Part A: Polym. Chem.*, 2008, **46**, 3512–3518.
13 A. Chernykh, T. Agag and H. Ishida, *Polymer*, 2009, **50**, 3153–3157.
14 Y. L. Liu and C. I. Chou, *J. Polym. Sci., Part A: Polym. Chem.*, 2005, **43**, 5267–5282.
15 R. Andreu, M. A. Espinosa, M. Galia, V. Cadiz, J. C. Ronda and J. A. Reina, *J. Polym. Sci., Part A: Polym. Chem.*, 2006, **44**, 1529–1540.
16 R. Kudoh, A. Sudo and T. Endo, *Macromolecules*, 2010, **43**, 1185–1187.
17 B. Kiskan, Y. Koz and Y. Yagci, *J. Polym. Sci., Part A: Polym. Chem.*, 2009, **47**, 6955–6961.
18 F. C. Wang, C. Y. Su, W. S. Kuo, F. C. Huang, Y. C. Sheen and F. C. Chang, *Angew. Chem., Int. Ed.*, 2006, **45**, 2248–2251.
19 W. S. Kuo, C. Y. Wu, F. C. Wang and U. K. Jeong, *J. Phys. Chem. C*, 2009, **113**, 20666–20673.
20 L. Qu and Z. Xin, *Langmuir*, 2011, **27**, 8365–8370.
21 F. C. Wang; C. F. Chang and W. S. Kuo *"Handbook of Polybenzoxazine"*, ed. Ishida, H. and Agag, T., Elsevier, Amsterdam 2011, ch. 33, p. 579.
22 H. C. Lin, L. S. Chang, Y. T. Shen, S. Y. Shih, T. H. Lin and F. C. Wang, *Polym. Chem.*, 2012, **3**, 935–945.
23 C. Y. Wu and S. W. Kuo, *Polymer*, 2010, **51**, 3948–3955.
24 A. Raza, Y. Si, X. Wang, T. Ren, B. Ding, J. Yu and S. S. Al-Deyab, *RSC Adv.*, 2012, **2**, 12804–12811.
25 S. C. Liao, F. C. Wang, C. H. Lin, Y. H. Chou and C. F. Chang, *J. Phys. Chem. C*, 2008, **112**, 16189–16191.
26 F. C. Wang, F. S. Chiou, H. F. Ko, K. J. Chen, T. C. Chou, F. C. Huang, W. S. Kuo and C. F. Chang, *Langmuir*, 2007, **23**, 5868–5871.
27 S. C. Liao, S. J. Wu, F. C. Wang and C. F. Chang, *Macromol. Rapid Commun.*, 2008, **29**, 52–56.
28 W. S. Kuo and W. C. Liu, *J. Appl. Polym. Sci.*, 2010, **117**, 3121–3127.
29 W. K. Huang and W. S. Kuo, *Polym. Compos.*, 2011, **32**, 1086–1089.
30 T. Takeichi, Y. Guo and T. Agag, *J. Appl. Polym. Sci.*, 2000, **38**, 4165–4176.
31 T. Takeichi and Y. Guo, *Polym. J.*, 2001, **33**, 437–443.
32 T. Takeichi, Y. Guo and S. Rimdusit, *Polymer*, 2005, **46**, 4909–4916.
33 Z. Brunovska and H. Ishida, *J. Appl. Polym. Sci.*, 1999, **73**, 857–862.
34 J. H. Kim, Z. Brunovska and H. Ishida, *Polymer*, 1999, **40**, 1815–1822.
35 Z. Brunovska, R. Lyon and H. Ishida, *Thermochim. Acta*, 2000, **357**, 195–207.
36 T. Agag and T. Takeichi, *Macromolecules*, 2001, **34**, 7257–7263.
37 T. Agag and T. Takeichi, *Macromolecules*, 2003, **36**, 6010–6017.
38 C. Y. Yen, C. C. Cheng, L. Y. Chu and C. F. Chang, *Polym. Chem.*, 2011, **2**, 1648–1653.
39 H. W. Hu, K. W. Huang and W. S. Kuo, *Polym. Chem.*, 2012, **3**, 1546–1554.
40 Y. Yagci, B. Kiskan, L. A. Demirel and O. Kamer, *J. Polym. Sci. Part A: Polym. Chem.*, 2008, **46**, 6780–6788.
41 K. D. Demir, M. A. Tasdelen, T. Uyar, A. W. Kawaguchi, A. Sudo, T. Endo and Y. Yagci, *J. Polym. Sci., Part A: Polym. Chem.*, 2011, **49**, 4213–4220.
42 K. H. Fu, F. C. Huang, W. S. Kuo, C. H. Lin, R. D. Yei and C. F. Chang, *Macromol. Rapid Commun.*, 2008, **29**, 1216–1220.
43 W. S. Kuo and C. F. Chang, *Prog. Polym. Sci.*, 2011, **36**, 1649–1696.
44 Q. Chen, R. Xu, J. Zhang and D. Yu, *Macromol. Rapid Commun.*, 2005, **26**, 1878–1882.
45 Y. Liu and S. Zheng, *J. Polym. Sci., Part A: Polym. Chem.*, 2006, **44**, 1168–1181.
46 M. J. Huang, W. S. Kuo, J. H. Huang, X. Y. Wang and Y. T. Chen, *J. Appl. Polym. Sci.*, 2009, **111**, 628–634.
47 H. W. Hu, W. K. Huang, W. C. Chiou and W. S. Kuo, *Macromolecules*, 2012, **45**, 9020–9028.
48 *"Handbook of Polybenzoxazine,"* ed. Xu, R.; Zhang, P.; Wang, J.; Yu, D.; Ishida, H. and Agag, T., Elsevier, Amsterdam 2011, ch. 31, p. 541.
49 C. C. Yang, I. P. Wang, C. Y. Lin, J. D. Liaw and W. S. Kuo, *Polymer*, 2014, **55**, 2044–2050.
50 F. Meng, H. Ishida and X. Liu, *RSC Adv.*, 2014, **4**, 9471–9475.
51 A. W. Kawaguchi, A. Sudo and T. Endo, *J. Polym. Sci., Part A: Polym. Chem.*, 2014, **52**, 410–416.
52 W. Szymanski, M. J. Beierle, V. A. H. Kistemaker, A. W. Velema and L. B. Feringa, *Chem. Rev.*, 2013, **113**, 6114–6178.
53 D. F. Jochum and P. Theato, *Chem. Soc. Rev.*, 2013, **42**, 7468–7483.
54 D. H. Kim and H. Ishida, *J. Phys. Chem. A*, 2002, **106**, 3271–3280.
55 W. Jiang, G. Wang, Y. He, X. Wang, Y. An, Y. Song and L. Jiang, *Chem. Commun.*, 2005, 3550–3552.
56 Y. H. Low and H. Ishida, *Polym. Degrad. Stab.*, 2006, **91**, 805–815.
57 O. T. Lekesiz and J. Hacaloglu, *Polymer*, 2014, **55**, 3533–3542.
58 W. S. Kuo, H. C. Wu and C. F. Chang, *Macromolecules*, 2004, **37**, 192–202.
59 T. A. Pires, C. Cheng and A. L. Belfiore, ACS. Proc. Div., *Polym. Mater.: Sci. Eng.*, 1989, **61**, 466.

60 W. S. Kuo, F. C. Huang, H. C. Wu and C. F. Chang, *Polymer*, 2004, **45**, 6613–6620.
61 C. Liu, D. Shen, M. R. Sebastian, J. Marquet and R. Schonfeld, *Macromolecules*, 2011, **44**, 4616–4622.
62 H. J. Wang, O. Altukhov, C. C. Cheng, C. F. Chang and W. S. Kuo, *Polymers.*, 2013, **5**, 937–953.